Nucleocytoplasmic Distribution of Rabies Virus P-Protein Is Regulated by Phosphorylation Adjacent to C-Terminal Nuclear Import and Export Signals†

Gregory W. Moseley,* Richard P. Filmer, Michelle A. DeJesus, and David A. Jans

Nuclear Signalling Laboratory, Department of Biochemistry and Molecular Biology, Monash University, Monash, Victoria 3800, Australia

Received March 15, 2007; Revised Manuscript Received July 2, 2007

ABSTRACT: Nucleocytoplasmic distribution of the rabies virus phosphoprotein is implicated in the evasion of cellular antiviral mechanisms by rabies virus and has been reported to depend on an N-terminal nuclear export sequence and a C-terminal nuclear localization sequence. This paper identifies a second nuclear export sequence that is located between key residues of the nuclear localization sequence in the phosphoprotein C-terminal domain. The C-terminal domain confers predominantly nuclear localization in unstimulated transfected cells, indicating that the nuclear localization sequence is the dominant signal at steady state. However, protein kinase-C activation or mutagenesis to mimic protein kinase-C phosphorylation at a site proximal to the C-terminal nuclear localization/export sequences shifts the targeting activity of the C-terminal domain toward nuclear exclusion, indicating that the nuclear export sequence becomes the dominant signal in activated cells. Mapping of these sequences within the three-dimensional structure of the C-terminal domain indicates that their activities may be coregulated by phosphorylation and/or conformational changes in the domain. The data are consistent with a model in which intimate positioning of the nuclear localization sequence, export sequence, and phosphorylation site within a single domain provides a switch mechanism to rapidly and efficiently balance the reciprocal import and export signals in response to cellular stimuli.

Nucleocytoplasmic protein trafficking is a key process in cellular development and physiology and is exploited by pathogens including viruses and plant bacteria (*1*−*4*). All transport into or out of the nucleus occurs through the nuclear membrane embedded nuclear pore complexes. For large molecules (>45 kDa), nuclear import/export requires active transport mediated by specific nuclear import (importins) or export (exportins including CRM-1) proteins (*5*, *6*). Importin and exportin interaction with cargoes is conferred by nuclear localization sequences (NLSs[1]) and nuclear export sequences (NESs), respectively, which are found in the cargo protein. These interactions can be dynamically regulated through specific mechanisms including phosphorylation and molecular masking/unmasking of NLSs/NESs in the cargo (*5*−*9*).

Interaction with the cellular nuclear import/export machinery is essential to the life cycle of most DNA viruses as well as retroviruses, which must deliver their genetic material to the nucleus for productive infection, but nuclear trafficking of various viral gene products is also common among viruses having cytoplasmic life cycles (*1*, *10*−*12*). The phospho (P-)protein of rabies virus (a negative-strand RNA virus of the lyssavirus genus) contains a CRM-1 exportin-dependent NES in its N terminus (designated here NES#1) and basic residues that are involved in nuclear import (K214, R260) by appearing to form part of a conformational NLS through their proximal location on the surface of the folded C-terminal domain (CTD) (Figure 1) (*11*). Nucleocytoplasmic localization of rabies P-protein (RPP) and other viral proteins has been implicated in the modulation of biological processes including apoptosis and interferon-induced antiviral responses (*11*, *13*, *14*).

RPP is one of only five proteins produced by the rabies virus, which implies that there is a requirement for multifunctionality/heterogeneity of the individual proteins to mediate the viral life cycle. RPP acts as a cofactor in RNA polymerase function of the rabies large (L)-protein and as a chaperone for the rabies nucleo (N)-protein (*13*), containing a single interaction site for L, one site for interaction with N, and another for N complexed with the viral RNA genome (N-RNA) (Figure 1) (*13*). Interaction of the RPP CTD with N-RNA results in the exposure of a masked antibody epitope in the CTD (*15*), presumably reflecting structural changes that may dynamically regulate RPP function. RPP also contains a dynein light chain association sequence (DLC-AS), which interacts with the dynein chain LC8 and facilitates RPP nuclear accumulation, as well as regions that interact with proteins relevant to the cellular antiviral response (Figure 1) (*13*, *16*−*18*). A leaky scanning mechanism produces four truncated RPP protein species (P2−

† This research was supported by the National Health and Medical Research Council, Australia (fellowship 384109 and project grant 384107).

* Author to whom correspondence should be addressed (telephone +61 3 9902 1312; fax +61 3 9905 3726; e-mail greg.moseley@med.monash.edu.au).

[1] Abbreviations: NLS, nuclear localization sequence; NES, nuclear export sequence; P-protein, phosphoprotein; CTD, C-terminal domain; RPP, rabies virus phosphoprotein; N-RNA, rabies virus N protein−RNA complex; DLC-AS, dynein light chain association sequence; PKC, protein kinase-C; CLSM, confocal laser scanning microscopy; LMB, leptomycin-B; PMA, phorbol myristyl acetate; Fn/c, ratio of nuclear to cytoplasmic fluorescence.

10.1021/bi700521m CCC: $37.00
Published on Web 10/09/2007

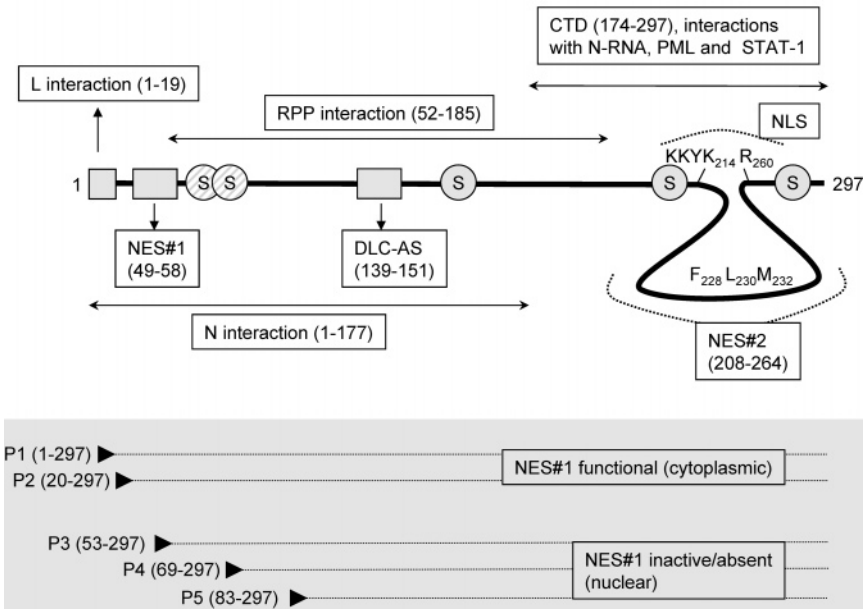

FIGURE 1: Schematic diagram of the RPP structure (P1, residues 1−297). Regions involved in forming intermolecular interactions are shown together with the PKC phosphorylation sites (S_{162}, S_{210}, S_{271}), which are shown as filled circles; other phosphorylation sites (S_{63}, S_{64}) are shown as hatched circles. Regions previously reported to be involved in determining the nucleocytoplasmic distribution of RPP (NLS, NES#1, and DLC-AS) are indicated. The position of NES#2 and key residues involved in NES#2 activity (identified in this study) are also shown. The lower panel shows the truncated RPP species, which are expressed in infected cells, and their nucleocytoplasmic distribution.

P5) in addition to full-length RPP (P1) in infected cells. These proteins differ in subcellular localization owing to the presence (P1, P2) or disruption/absence (P3−5) of NES#1 (Figure 1) (*11*). RPP is also phosphorylated at multiple sites by protein kinase-C (PKC) and another cellular kinase (Figure 1) (*19*). Thus, RPP produces multiple heterogeneous protein species to perform a number of functions during rabies infection, these requiring differential localization of RPP to the nuclear and cytoplasmic compartments.

Here we report the first quantitative study of nuclear localization of RPP, which identifies a second CRM-1-dependent NES (NES#2) in the RPP CTD. NES#2 is closely associated with residues reported to form the NLS. NES#2 is functional in P3 protein, in which NES#1 is reported to be inactivated by truncation (*11*) and which has been suggested to play key roles in modulating the cellular antiviral response (*11*, *13*). Nucleocytoplasmic trafficking appears to be regulated by a PKC phosphorylation site proximal to both NES#2 and the NLS. Consideration of the structural organization of the NES, NLS, and PKC phosphorylation site in the CTD indicates that PKC activity could simultaneously regulate both import and export signals to balance nucleocytoplasmic localization of RPP. We hypothesize that the CTD acts as a novel molecular switch to regulate trafficking of RPP.

EXPERIMENTAL PROCEDURES

Constructs. The plasmid pLex-P containing full-length RPP was kindly supplied by D. Blondel (Unite Mixté de Virologie Moléculaire et Structurale, Gif sur Yvette Cedex, France). PCR was used to produce fragments containing RPP P1 (full length, RPP_{1-297}, position of amino acids in protein sequence shown in subscript), RPP P3 (RPP_{54-297}), RPP CTD ($RPP_{174-297}$), $RPP_{208-264}$, and $RPP_{262-297}$ flanked by *Bgl*II sites at the 5′ and 3′ ends. The inserts were digested with *Bgl*II and cloned into the pEGFP-C1 plasmid to produce constructs for expression of GFP-RPP P1, GFP-RPP P3, GFP-RPP CTD, GFP-$RPP_{208-264}$, and GFP-$RPP_{262-297}$ fusion proteins in mammalian cells.

The NLS from human cytomegalovirus (hCMV) ppUL44 protein was produced by PCR from the pDEST53-UL44C2N vector (*20*) to amplify the coding sequence for residues 421−433, which introduced *Bam*HI and *Bgl*II restriction sites at the 5′ and 3′ ends, respectively; these sites were flanked by Gateway recombination sites. The PCR fragment was cloned into the mammalian expression vector pEPI-GFP-DESTC (*12*) by recombination using Gateway cloning technology (Invitrogen, Carlsbad, CA) in frame C-terminal to the reading frame of GFP to produce the vector pEPI-GFP-UL44 NLS. The sequence encoding $RPP_{221-238}$ was PCR amplified to introduce *Bam*HI and *Bgl*II sites at the 5′ and 3′ ends and was inserted by *Bam*HI/*Bgl*II cloning (*18*, *21*) into the unique *Bgl*II site 3′ of the UL44 NLS in the pEPI-GFP-UL44 NLS vector, in frame with UL44 NLS, to produce pEPI-GFP-UL44 NLS-$RPP_{221-238}$. These constructs produce GFP-UL44 NLS and GFP-UL44 NLS-$RPP_{221-238}$ fusion proteins when expressed in mammalian cells.

Site-directed mutagenesis of proteins was performed using the overlap PCR technique (*22*). The PKC-α-eGFP encoding construct was from Clontech. The plasmid encoding GFP fused to the HIV REV NES and NLS has been described previously (*23*, *24*).

Transfections and Drug Treatments. For transfection, COS-7 cells were grown to 80% confluency on coverslips in DMEM with 10% FCS in 5% CO_2 at 37 °C. Transient transfection was performed using Lipofectamine 2000 (Invitrogen) according to the manufacturer's instructions, and cells were analyzed by confocal laser scanning microscopy (CLSM, see below) 18−24 h post-transfection. For inhibition of CRM-1-mediated nuclear export, leptomycin-B (LMB) was added to the media to a final concentration of 2.8 ng/mL 3 h before CLSM analysis. For PKC activation, phorbol

myristyl acetate (PMA) was added to the media to a final concentration of 1 μM 1 h prior to analysis.

CLSM Analysis. Imaging of live cells was performed using a Bio-Rad MRC-600 CLSM with a 40× water immersion objective and heated stage (*20*, *25*, *26*). Analysis of digitized confocal files used Image J 1.62 public domain software (NIH), calculating fluorescence intensity for the nucleus (Fn) and cytoplasm (Fc), which were corrected for background fluorescence and used to calculate the Fn/c ratio as previously described (*18*, *27*, *28*). Graph Pad Instat software was used for statistical analysis.

To calculate the cellular fluorescence intensity of transfected cells corrected for background fluorescence intensity, the mean nuclear fluorescence with background fluorescence intensity subtracted (Fn) and the mean cytoplasmic fluorescence with background fluorescence intensity subtracted (Fc) were calculated for >50 images of transfected cells using Image J 1.62 software (*18*); cellular fluorescence was calculated as Fn + Fc.

Structure Analysis. The PDB file of the RPP CTD crystal structure (*29*) was obtained from the National Centre for Biotechnology database, and structural analysis used the PyMol Molecular Graphics System software (W. L. DeLano, 2002, DeLano Scientific, San Carlos, CA). Representations of surface potential were produced using the CCP4 molecular graphics software (*30*).

RESULTS

Identification of a NES in the RPP CTD. RPP produces five protein species in infected cells (full-length protein [P1] and truncated proteins [P2−P5]) owing to translation from internal methionines (*11*, *31*). Proteins containing NES#1 (P1 and P2, which are initiated at Met1 and Met 20, respectively) have been reported to be excluded from the nucleus with dependence on CRM-1 activity, whereas truncated proteins in which NES#1 is disrupted/absent (P3, P4, and P5, initiated at Met 53, Met 69, and Met 83, respectively) accumulate in the nucleus due to nuclear localizing activity in the CTD (Figure 1) (*11*). However, the nuclear import/export of RPP has not previously been assessed quantitatively.

To quantitatively examine nuclear transport of RPP proteins P1 and P3 (RPP_{54-297}) and the RPP CTD ($RPP_{174-297}$), we cloned the coding sequences for these proteins in frame C-terminal to the reading frame of GFP in the vector pEGFP-C1. As the fusion proteins start translation at the GFP start codon and read into the P protein sequence, the internal AUG start codon of P3 (M_{53}) was deleted from the sequence, so GFP-P3 contains RPP amino acid residues 54−297 rather than 53−297. These fusion proteins were expressed in COS-7 cells for analysis by CLSM, with nuclear localization quantified by calculating the ratio of nuclear to cytoplasmic fluorescence intensity (Fn/c) as described under Experimental Procedures. As can be seen in Figure 2, GFP-RPP P1 was excluded from the nucleus, whereas GFP-RPP P3 and GFP-RPP CTD accumulated in the nucleus to a greater level than GFP alone, which is consistent with previous observations described above (*11*). P1 contains NES#1 (*11*) and, as expected, nuclear export was significantly inhibited by treatment with LMB (Figure 2), a specific inhibitor of CRM-1-mediated nuclear export. Intriguingly, although P3 is truncated within NES#1 and the CTD entirely lacks the

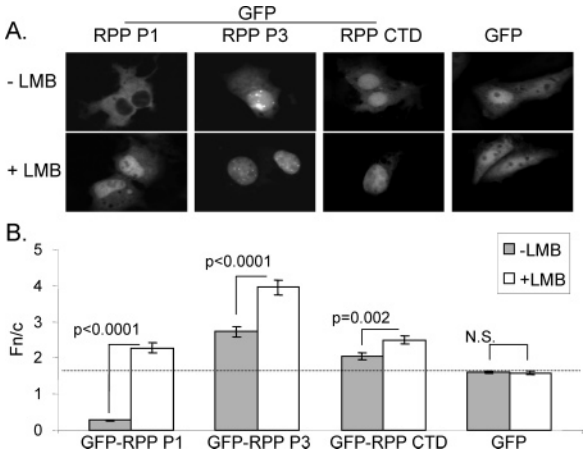

FIGURE 2: Nuclear localization conferred by the RPP CTD is responsive to LMB. (A) COS-7 cells were transfected to express the indicated GFP-fusion protein and analyzed by CLSM 18−24 h later; where indicated, LMB was added to cells to a final concentration of 2.8 ng/mL 3 h prior to CLSM. (B) Images such as those shown in (A) were analyzed to calculate the ratio of nuclear to cytoplasmic fluorescence (Fn/c). Nuclear accumulation of both GFP-RPP P3 and GFP-RPP CTD is greater than that of GFP alone (highlighted by dotted line), whereas GFP-RPP P1 shows significant nuclear exclusion. Nuclear localization of the RPP P1-, P3-, and CTD-containing proteins is significantly increased upon treatment with LMB. The negative control, GFP alone, is unaffected by LMB treatment. Results are shown as the mean ± SEM for $n > 50$.

NES#1 sequence, both GFP-RPP P3 and GFP-RPP CTD showed significant increases in nuclear accumulation upon LMB treatment (Figure 2). GFP alone showed no effect of LMB treatment on nuclear localization, demonstrating that the observed effects of LMB were entirely dependent on the RPP sequences fused to GFP (Figure 2). Nuclear export of the HIV-1 REV protein is known to use the CRM-1-mediated export pathway (*32*), and nuclear accumulation of a GFP fusion protein containing the REV NES and NLS (*23*, *24*) was significantly enhanced by this LMB treatment (not shown). Thus, it appeared that RPP contains a second CRM-1-dependent NES (NES#2) within the CTD.

Identification of NES#2 Sequence. To further characterize the mechanisms of nuclear import/export of RPP, we produced GFP-$RPP_{208-264}$, which contains residues shown previously to be essential for nuclear accumulation of RPP (K_{214}, R_{260}) (Figure 3A, upper panel) (*11*), and nuclear localization of this protein was assessed as described above. Intriguingly, rather than accumulating in the nucleus of transfected cells, GFP-$RPP_{208-264}$ showed clear nuclear exclusion (Figure 3B). $RPP_{208-264}$ contains a number of hydrophobic residues that could form a CRM-1-dependent NES (Figure 3A, upper panel, and see below). We found that a second fragment of the CTD, $RPP_{262-297}$, which contains a similar proportion of hydrophobic residues as $RPP_{208-264}$ (Figure 3A), did not cause nuclear exclusion of fused GFP compared with GFP alone (Figure 3B). This indicated that nuclear export activity conferred by the truncated protein $RPP_{208-264}$ is due to a specific sequence in this region.

To test whether nuclear export mediated by $RPP_{208-264}$ was due to CRM-1 activity, we examined the effect of LMB treatment on the subcellular distribution of GFP-$RPP_{208-264}$, finding that treatment significantly increased nuclear localization (Figure 3C,D). Thus, GFP-$RPP_{208-264}$ appeared to

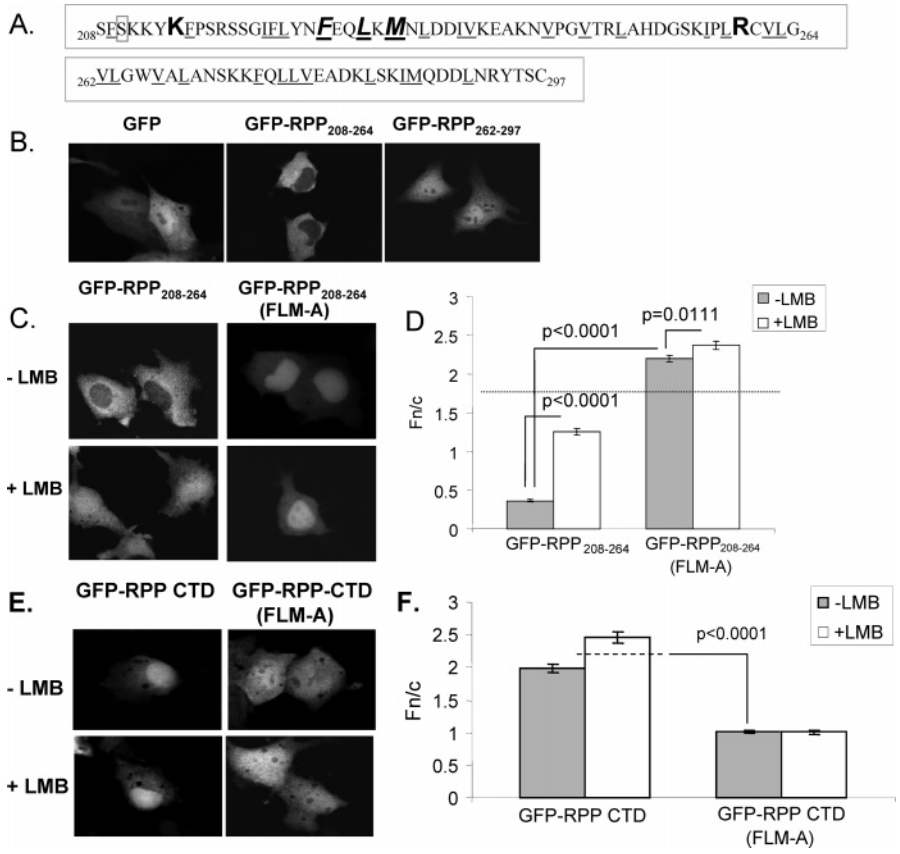

FIGURE 3: Characterization of RPP NES#2. (A) The primary sequences of $RPP_{208-264}$ (upper panel) and $RPP_{262-297}$ (lower panel) are shown. Hydrophobic residues are underlined, residues selected for mutation to alanine (F_{227}, L_{230}, M_{232}) are shown in large bold italics, residues reported to be involved in nuclear accumulation (K_{214}, R_{260}) are shown in large bold type, and the S_{210} PKC phosphorylation site is boxed. (B, C, E) COS-7 cells were transfected to express the indicated protein and analyzed as described in the caption of Figure 2. (B) GFP-$RPP_{208-264}$ is clearly excluded from the nucleus, but GFP-$RPP_{262-297}$ is diffusely distributed, similar to GFP alone. (C) CLSM images show that nuclear export of GFP-$RPP_{208-264}$ is inhibited by LMB treatment or mutation of potential NES#2 residues (shown in (A), upper panel) to produce GFP-$RPP_{208-264}$(FLM-A), and (D) image analysis shows that the increases in nuclear localization are highly significant. Nuclear accumulation of GFP-$RPP_{208-264}$(FLM-A) is greater than that of GFP alone (shown as dotted line) and shows a considerable reduction in sensitivity to LMB treatment compared with GFP-$RPP_{208-264}$. (E) GFP-RPP CTD(FLM-A) is diffusely distributed in transfected cells compared with GFP-RPP CTD, which localizes in the nucleus, and (F) image analysis shows that nuclear accumulation of GFP-RPP CTD(FLM-A) is significantly inhibited compared with GFP-RPP CTD and is insensitive to LMB treatment. Results are shown as the mean ± SEM for $n > 50$.

contain an active CRM-1-dependent NES, which caused nuclear exclusion in the absence of LMB. This contrasted with larger RPP proteins (RPP CTD and RPP P3), which mediated accumulation in the nucleus in the absence of LMB (Figure 2). The intact CTD forms a compact domain in which many of the hydrophobic residues will be buried (see Discussion). Thus, it appeared that the expression of the short fragment $RPP_{208-264}$ had exposed a NES which was partially obscured in the context of the intact CTD structure when expressed in unstimulated cells.

CRM-1-dependent NESs commonly conform to the motif LxxLxL, where L can be the hydrophobic residue L, I, V, F, or M (*7*). Examination of the sequence of $RPP_{208-264}$ identified a cluster of hydrophobic residues that could form NES#2 (Figure 3A, upper panel). We selected F_{227}, L_{230}, and M_{232} for mutational substitution to alanine in the $RPP_{208-264}$ sequence, producing $RPP_{208-264}$(FLM-A). Analysis of cells transfected with GFP-$RPP_{208-264}$(FLM-A) showed that this mutation resulted in a significant increase in nuclear accumulation compared with GFP-$RPP_{208-264}$, which was accompanied by a considerably diminished sensitivity to LMB, confirming that these mutations had disrupted NES#2 activity in $RPP_{208-264}$ (Figure 3C,D). Interestingly, GFP-$RPP_{208-264}$(FLM-A) accumulated in the nucleus to a greater extent than GFP alone (Figure 3D). Thus, nuclear import activity appears to be retained to some extent in $RPP_{208-264}$-(FLM-A), with the NLS becoming the dominant targeting signal when NES#2 is disabled.

The FLM-A mutation was also introduced into GFP-RPP CTD. We observed that nuclear accumulation of GFP-RPP CTD(FLM-A) was insensitive to LMB treatment, indicating that NES#2 activity had been disabled (Figure 3E,F). However, nuclear localization of GFP-RPP CTD(FLM-A) was significantly lower than that of wild type GFP-RPP CTD, indicating that NLS activity had also been disabled (Figure 3E,F). Mutation of Mokola lyssavirus P-protein to convert M_{233} (which corresponds to the conserved M_{232} in RPP) to a threonine was reported previously to affect the P-protein interaction with Mokola virus N-protein (*33*). It has been predicted that this mutation would result in destabilization of core packing of the globular RPP CTD (*29*). It is possible, therefore, that the FLM-A mutation affects the global structure of the intact CTD, resulting in deactivation of the NES and the NLS. Thus, although the FLM-A mutation was useful for mapping the functional NES#2 when the CTD was substantially truncated in the form of $RPP_{208-264}$,

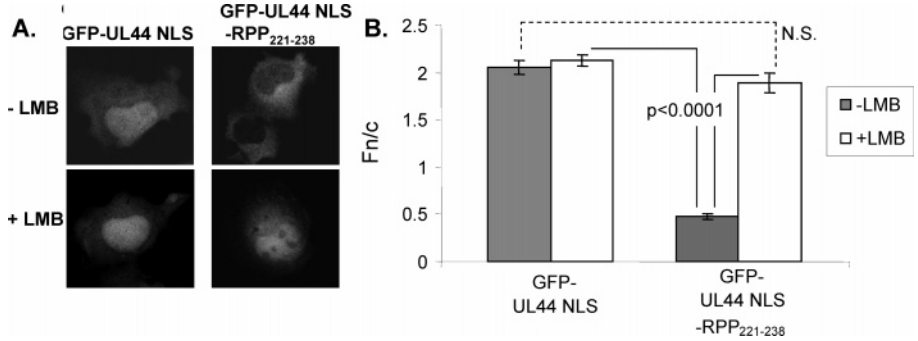

FIGURE 4: RPP NES#2 can act as an independent module to cause nuclear exclusion of a heterologous NLS. Cells were transfected to express the indicated proteins and analyzed with or without treatment with LMB as described in the caption of Figure 2. (A) GFP−UL44 NLS shows nuclear accumulation with or without LMB treatment, whereas GFP−UL44 NLS−$RPP_{221-238}$ is clearly excluded from the nucleus without LMB, but accumulates in the nucleus following LMB treatment. (B) Image analysis confirmed that GFP−UL44 NLS accumulates in the nucleus, and nuclear localization is unaffected by LMB treatment, whereas the GFP−UL44 NLS−$RPP_{221-238}$ fusion protein shows significant nuclear exclusion compared with GFP−UL44 NLS. Following LMB treatment GFP−UL44 NLS−$RPP_{221-238}$ accumulates in the nucleus to a level not significantly different from that of GFP−UL44 NLS. Results are shown as the mean ± SEM for $n > 40$.

this mutation was not investigated further in the context of the intact CTD or larger RPP proteins.

RPP NES#2 Can Act Independently To Regulate Nuclear Targeting by a Heterologous NLS. Having identified key residues involved in the CRM-1-dependent export of $RPP_{208-264}$, we next tested whether a considerably truncated RPP sequence containing residues representing a minimal NES sequence, and lacking the RPP NLS residues (K_{214}, R_{260}), could mediate nuclear export as an independent module and cause relocalization of a heterologous NLS to the cytoplasm. The LxxLxL is a minimal motif, and functional NESs will require additional flanking residues (*34*); therefore, to produce a minimal functional RPP NES, we selected the sequence $RPP_{221-238}$, which contains the six residues that form the LxxLxL motif (F_{227}−M_{232}) and the six N-terminal and six C-terminal residues that flank this motif. For a heterologous NLS we used the UL44 NLS (residues 421−433 of hCMV ppUL44 (*20*)), which contains a short, basic NLS sequence (PNTKKQK) that is imported to the nucleus via the classical import pathway involving the α/β importin heterodimer (*20*). The UL44 NLS acts as a module conferring nuclear accumulation to GFP when GFP-UL44 NLS fusion protein is expressed in mammalian cells (Figure 4). To test the ability of $RPP_{221-238}$ to cause nuclear export of the GFP−UL44 NLS fusion protein, we produced a construct that expresses GFP, UL44 NLS, and $RPP_{221-238}$ as a single fusion protein with the NLS and putative RPP NES expressed in tandem (GFP−UL44 NLS−$RPP_{221-238}$). As can be seen in Figure 4, the attachment of $RPP_{221-238}$ to the UL44 NLS results in clear nuclear export of the protein in transfected cells. The nuclear localization of GFP−UL44 NLS was unaffected by LMB treatment (Figure 4B), confirming the absence of NES activity in the GFP or UL44 NLS sequences; however, LMB caused a significant increase in nuclear accumulation of GFP−UL44 NLS−$RPP_{221-238}$ (Figure 4B). The nuclear accumulation of GFP−UL44 NLS−$RPP_{221-238}$ in LMB-treated cells was not different from accumulation of GFP−UL44 NLS in untreated cells (Figure 4B). Thus, the UL44 NLS is functional in the context of both fusion proteins, and the predominantly cytoplasmic localization of GFP−UL44 NLS−$RPP_{221-238}$ in untreated cells is due to nuclear export driven by a CRM-1-dependent NES in the $RPP_{221-238}$ fragment, demonstrating that RPP contains a modular NES in the CTD within residues 221−238.

Regulation of CTD Nuclear Accumulation by Phosphorylation. In vitro phosphorylation studies suggest that PKC phosphorylates RPP at three sites which conform to the S/T−X−K/R consensus PKC phosphorylation site (S_{162}, S_{210}, and S_{271}) (*19*). The PKC site serine S_{210} is located next to the predicted NLS residues $KKYK_{214}$ in the primary sequence of RPP (Figure 3A, upper panel) and adjacent to a patch of positive potential on the surface of the CTD, which includes the residues K_{214} and R_{260} that are required for RPP nuclear import (*11*, *29*). No functional effect has previously been attributed to S_{210} phosphorylation, but the functions of NLSs and NESs are commonly regulated by phosphorylation (*5*, *6*).

To examine whether PKC phosphorylation might affect NLS/NES#2 activity, we first tested the effect of the PKC agonist PMA on RPP nucleocytoplasmic distribution. Treatment of cells transfected to express GFP-RPP P3 or GFP-RPP CTD with PMA produced a significant inhibition of nuclear localization, implying that PKC activation shifted the CTD from nuclear import toward nuclear export (Figure 5). The effect of PMA could be inhibited by LMB treatment, resulting in significantly increased nuclear localization of GFP-RPP P3 and GFP-RPP CTD in cells treated with LMB and PMA compared with PMA alone (Figure 5). Thus, the altered nuclear accumulation appears to involve CRM-1 activity. Treatment of cells transfected to express GFP-PKCα with PMA resulted in relocalization of GFP-PKCα from the cytoplasm to membrane structures as expected, confirming the efficacy of this PMA treatment to activate PKC (not shown).

As PMA can produce pleiotropic cellular effects, we next examined the effect of modification of S_{210} directly. S_{210} in the RPP CTD was mutated to alanine (RPP CTD(S_{210}A)) and aspartic acid (RPP CTD(S_{210}D)), and these sequences were cloned into pEGFP-C1 as above. The alanine-substituted derivative cannot be phosphorylated, whereas the aspartic acid derivative possesses a negative charge at S_{210}, which mimics a constitutively phosphorylated state. Expression of GFP-RPP CTD(S_{210}A) produced nuclear accumulation not different from that of GFP-RPP CTD, but GFP-

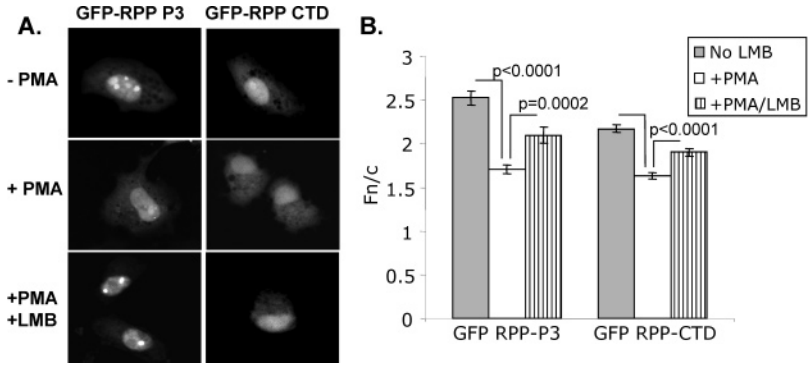

FIGURE 5: PKC activation affects nuclear localization of RPP. (A) Cells were transfected to express the indicated proteins and analyzed as described in the caption of Figure 2, with or without treatment with 2.8 ng/mL LMB for 3 h and/or 1 μM PMA for 1 h prior to CLSM. (B) Image analysis shows that nuclear localization of both GFP-RPP P3 and GFP-RPP CTD is significantly decreased by PMA treatment and that LMB treatment significantly inhibits this effect. Results are shown as the mean ± SEM for $n > 50$.

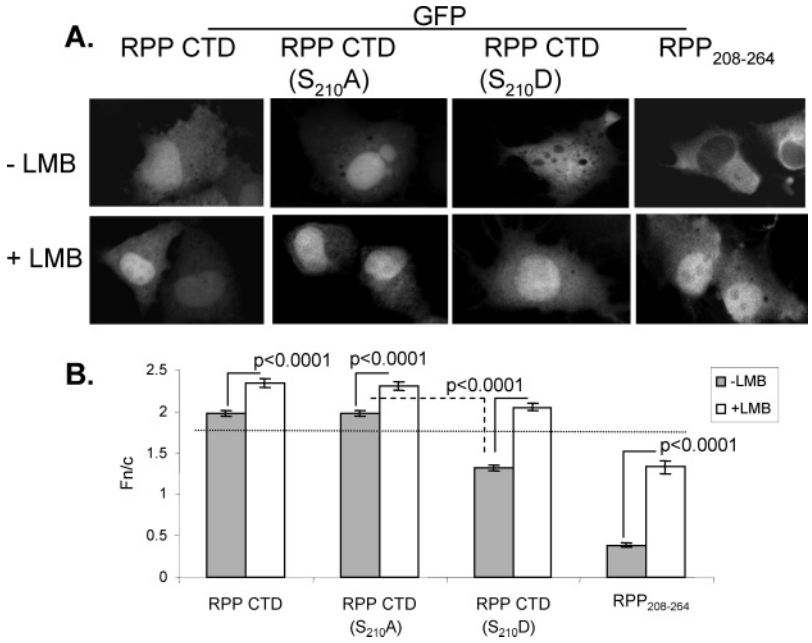

FIGURE 6: PKC phosphorylation site S_{210} affects nuclear import/export of the RPP CTD with dependence on CRM-1. (A) Cells were transfected to express the indicated protein and analyzed as described in the caption of Figure 2. (B) Image analysis revealed that nuclear accumulation of GFP-RPP CTD(S_{210}A) does not differ significantly from GFP-RPP CTD in cells treated with and without LMB, and both proteins show nuclear accumulation greater than that of GFP alone (shown as a dotted line). Nuclear localization of GFP-RPP CTD(S_{210}D) is decreased to a level lower than that of GFP alone (shown as dotted line). The nuclear accumulation of GFP-RPP CTD(S_{210}D) is significantly increased by LMB treatment. Results are shown as the mean ± SEM for $n > 50$.

RPP CTD(S_{210}D) was consistently less nuclear than GFP-RPP CTD or GFP protein alone (Figure 6). When treated with LMB, GFP-RPP CTD(S_{210}D) became significantly more nuclear, showing that nuclear distribution of this protein was dependent on CRM-1 activity (Figure 6). To confirm that the mutated proteins (RPP CTD(S_{210}A), RPP CTD(S_{210}D)) expressed at levels similar to that of the wild type protein, we calculated the mean cellular fluorescence intensity corrected for background for the transfected cell populations as described under Experimental Procedures, finding that mean fluorescence intensity for cells expressing GFP-RPP CTD, GFP-RPP CTD(S_{210}D), and GFP-RPP CTD(S_{210}A) was 187.6, 192.3, and 205.0, respectively, so the mean cellular fluorescence intensity did not differ by >9.2%; the fluorescence intensity of cells expressing GFP-P3 (186.9) was also within this range.

Thus, it appears that phosphorylation at S_{210} causes a shift in the competing activities of the NLS/NES targeting sequences to reduce nuclear accumulation of the protein.

DISCUSSION

In this study we identify a CRM-1-dependent NES (NES#2) in the C terminus of RPP for the first time. We show that nuclear localization of truncated RPP, in which the previously identified N-terminal NES (NES#1) has been disrupted or removed, is determined by the reciprocal activities of the newly discovered NES#2 and the NLS and can be regulated by phosphorylation at a proximal PKC site. The NLS, NES#2, and PKC phosphorylation sites are found closely associated in a single globular domain at the C terminus of RPP. Our data indicate that juxtapositioning of these sequences in a single domain provides an efficient molecular mechanism by which RPP can simultaneously regulate the opposing signals to shift the balance between nuclear export and import.

The sequence containing key RPP NES#2 residues (N**F**EQ**L**K**M**) conforms to the loosely conserved NES motif LxxLxL (where L is L, M, F, I, or V), which typically

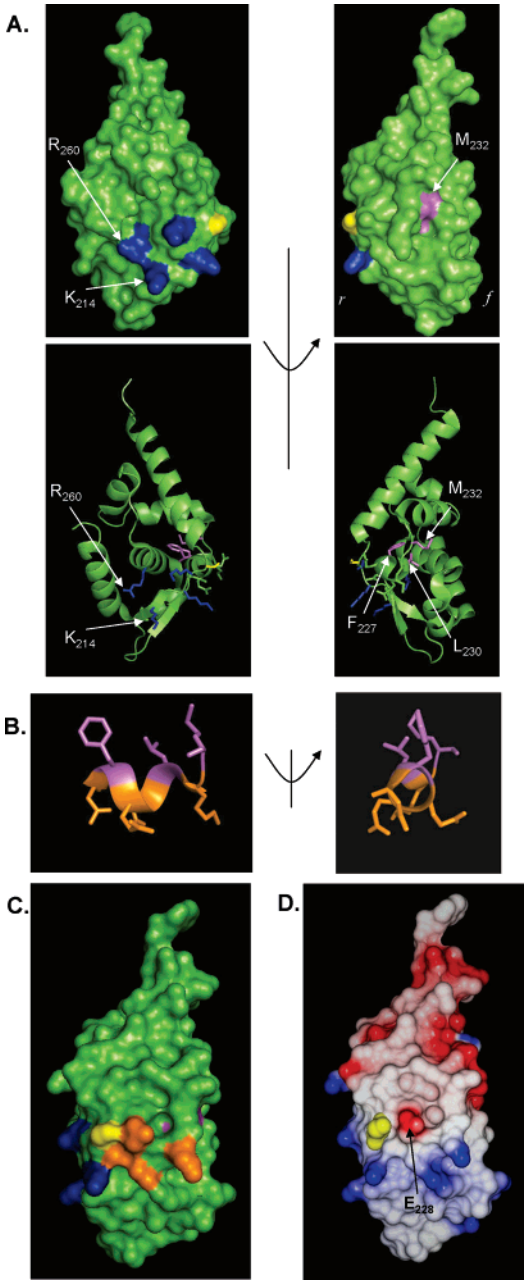

FIGURE 7: Location of NES#2, NLS, and S_{210} residues in the 3D structure of the RPP CTD monomer. (A) Surface representations (upper panel) and corresponding ribbon diagrams of secondary structure with side chains represented as sticks (lower panel) of the RPP CTD, residues 186−297. The left panel shows a front view of the round face of the CTD, and the right panel shows the view rotated 90° with the flat face (*f*) and round face (*r*) indicated. Of the side chains of the hydrophobic NES#2 residues (side chains shown in magenta), M_{232} is only partially exposed, L_{230} is oriented toward the CTD interior, and F_{227} is buried. The side chains of the basic residues implicated in NLS activity (K_{211}, K_{212}, K_{214}, and R_{260}, shown in blue) and the PKC phosphorylation site (S_{210}, side chain in yellow) are exposed on the surface of the round face. (B) Ribbon diagrams of the 3_{10} amphipathic helical structure of the NES region viewed from the side (left panel) and end (right panel) of the helix show that the hydrophobic residues (F_{227}, L_{230}, M_{232}, shown in magenta) and charged/polar residues (N_{226}, E_{228}, Q_{229}, K_{231}, shown in orange) emerge from opposite sides of the helix. (C) Surface representation of the RPP CTD shows that the NES#2 hydrophilic side chains (in orange) are surface exposed and proximal to S_{210} (in yellow). (D) CTD surface potential representation (with positive potential shown in blue and negative potential in red) shows that S_{210} (in yellow) is adjacent to the negative surface potential produced by E_{228}.

contains several charged residues (*7*). A more extensive NES consensus sequence (L-x(2,3)-[LIVFM]-x(2,3)-L-x-[LI]) has been predicted (*35*), and it is likely that NES#2 activity involves one or more of the neighboring hydrophobic residues in the CTD, but mutation of F_{227}, L_{230}, and M_{232} is clearly sufficient to inhibit nuclear export. The crystal structure of the CTD (residues 186−297) has been solved (*29*), allowing us to map these NES#2 residues in the domain (Figure 7). A key observation from mapping the NES is that the hydrophobic residues are oriented to the interior of the CTD structure: F_{227} is buried in the CTD core, L_{230} is oriented to the inside, and M_{232} is only partially exposed (Figure 7A). NES#2 contains an amphipathic 3_{10} helical structure (Figure 7B) (*11*, *29*), so that the hydrophilic residues (N_{226}, E_{228}, Q_{229}, K_{231}), which emerge from the opposite side of the helix to F_{227}, L_{230}, and M_{232}, are exposed at the CTD surface (Figure 7B,C), with E_{228} forming negative surface potential (Figure 7D). Consideration of the sequence/structure of known NESs indicates a tendency to form amphipathic α-helices (*7*), and the RPP NES#1 is predicted to be α-helical at residues 52−56 (*11*, *29*). Thus, NES#2 is similar to conventional NESs but differs in the helical structure it forms.

The export activity of certain NESs is known to be regulated by molecular masking/unmasking and/or phosphorylation (*5*−*9*, *36*, *37*), and our data are consistent with both forms of regulation playing a role in NES#2 activity. The inward orientation of the NES#2 hydrophobic residues (Figure 7A) suggests that they will not be readily accessible to CRM-1 unless the CTD undergoes some conformational change. It is notable that although P3 and RPP CTD both accumulate in the nucleus of transfected cells in the absence of LMB, the shorter fragments, $RPP_{208-264}$ and $RPP_{221-238}$, cause pronounced nuclear exclusion, suggesting that the NES is activated/exposed in these truncated proteins. Furthermore, the fact that functional NES activity is maintained by the 18-residue $RPP_{221-238}$ fragment demonstrates that the RPP NES is a short, independent targeting module. These data are consistent with observations made in other proteins where masked NESs have been exposed by truncation of the holoprotein (*36*, *38*, *39*). The nuclear exclusion seen for $RPP_{208-264}$ could not be directly attributed to deactivation of RPP NLS activity as $RPP_{208-264}$ still showed significant nuclear accumulation (comparable to that of the RPP CTD) when the NES#2 was inactivated by mutation. Thus, it appears that NES#2 represents a strong export signal, but may be negatively regulated by conformational restraints in RPP CTD and RPP P3 at steady state.

That the RPP CTD structure can be dynamically regulated is suggested by the exposure of a masked epitope in the CTD upon N-RNA interaction (*15*). The CTD mediates interactions of RPP with several other proteins (*13*), which could produce similar effects. As the spatial proximity of key residues involved in nuclear import (K_{214}, R_{260}) is dependent on the conformation of the CTD (*11*, *29*) and these residues flank the NES#2 residues in the RPP primary sequence, it is an intriguing possibility that conformational changes that expose NES#2 could also affect the NLS, thus counterbalancing NES#2/NLS activity and producing rapid, efficient switching between nuclear import and export. It is also of interest that the residues $KKYK_{214}$ are predicted to be involved in interaction with N-RNA as well as in NLS activity (*11*, *29*), so it is possible that certain intermolecular

interactions could mask/unmask nuclear transport signals both by intermolecular steric hindrance and by induction of intramolecular conformational changes.

Our data indicate that PKC phosphorylation at S_{210} switches the CTD from a configuration where the NLS is dominant to one where NES#2 is dominant, thus biasing RPP CTD localization from the nucleus to the cytoplasm. S_{210} is exposed on the CTD round face, adjacent to a region of positive surface potential produced by residues including K_{214}/R_{260}, which are necessary for nuclear import (Figure 7A) (*11*, *29*). It is likely that a negative phosphate group at S_{210} would affect the positive patch, diminishing the ability of the NLS residues to mediate nuclear import (*11*, *29*). Intriguingly, the hydrophilic residues of the NES#2 helix are also proximal to S_{210} on the CTD surface so that S_{210} is immediately adjacent to the negative surface potential produced by E_{228} (Figure 7C,D). It has been suggested that the exposed charged residues of NES helices may be important in initial interaction with CRM-1, this preceding local conformational change to permit interaction of CRM-1 with buried hydrophobic residues (*7*). It is possible that phosphorylation will have some influence on NES#2 activity, either by directly affecting the conformation/exposure of the hydrophobic NES residues or by affecting the interaction of CRM-1 with the CTD surface exposed hydrophilic NES residues. Thus, phosphorylation has the potential to affect nuclear import and export activity in concert.

Although the precise role of phosphorylation in RPP biology is unclear, it appears that the nucleocytoplasmic distribution of RPP protein species is regulated by PKC activation, providing a mechanism whereby rabies virus can detect and respond to changes in the cellular environment. One relevant case may be the activation of PKC in response to interferon, as RPP P1 and P3 are suggested to play key roles at several stages in rabies virus evasion of cellular antiviral mechanisms, this involving a number of distinct activities localized specifically in the nucleus or the cytoplasm (*13*).

In conclusion, we have shown that the closely associated NLS, NES#2, and S_{210} phosphorylation sites of RPP collaborate to control the nucleocytoplasmic distribution of RPP. Other than these CTD-localized sequences, the N-terminal NES#1 and centrally located DLC-AS also affect nuclear localization (*11*, *18*). Thus, RPP contains a series of distinct targeting signals that must be coordinated to produce the appropriate subcellular distribution, this involving regulation by mechanisms including truncation and phosphorylation. All of these targeting signals are highly conserved in the lyssavirus genus, indicating that these mechanisms of regulated trafficking are common among lyssaviruses and highlighting the importance of finely regulated nuclear import/export of P-proteins during lyssavirus infection.

ACKNOWLEDGMENT

We acknowledge Gus Fenalti for assistance with production of the surface potential representations and Danielle Blondel for supplying the pLex-P plasmid.

REFERENCES

1. Rawlinson, S. M., Pryor, M. J., Wright, P. J., and Jans, D. A. (2006) Dengue virus RNA polymerase NS5: a potential therapeutic target?, *Curr. Drug Targets 7*, 1623−38.
2. Piller, S. C., Caly, L., and Jans, D. A. (2003) Nuclear import of the pre-integration complex (PIC): the Achilles heel of HIV?, *Curr. Drug Targets 4*, 409−29.
3. Hearps, A. C., and Jans, D. A. (2006) HIV-1 integrase is capable of targeting DNA to the nucleus via an importin α/β-dependent mechanism, *Biochem. J. 398*, 475−84.
4. Citovsky, V., Guralnick, B., Simon, M. N., and Wall, J. S. (1997) The molecular structure of agrobacterium VirE2-single stranded DNA complexes involved in nuclear import, *J. Mol. Biol. 271*, 718−27.
5. Jans, D. A., Xiao, C. Y., and Lam, M. H. (2000) Nuclear targeting signal recognition: a key control point in nuclear transport?, *Bioessays 22*, 532−44.
6. Poon, I. K., and Jans, D. A. (2005) Regulation of nuclear transport: central role in development and transformation?, *Traffic 6*, 173−86.
7. la Cour, T., Kiemer, L., Molgaard, A., Gupta, R., Skriver, K., and Brunak, S. (2004) Analysis and prediction of leucine-rich nuclear export signals, *Protein Eng., Des. Sel. 17*, 527−36.
8. Stommel, J. M., Marchenko, N. D., Jimenez, G. S., Moll, U. M., Hope, T. J., and Wahl, G. M. (1999) A leucine-rich nuclear export signal in the p53 tetramerization domain: regulation of subcellular localization and p53 activity by NES masking, *EMBO J. 18*, 1660−72.
9. Wood, M. J., Storz, G., and Tjandra, N. (2004) Structural basis for redox regulation of Yap1 transcription factor localization, *Nature 430*, 917−21.
10. Kapoor, M., Zhang, L., Ramachandra, M., Kusukawa, J., Ebner, K. E., and Padmanabhan, R. (1995) Association between NS3 and NS5 proteins of dengue virus type 2 in the putative RNA replicase is linked to differential phosphorylation of NS5, *J. Biol. Chem. 270*, 19100−6.
11. Pasdeloup, D., Poisson, N., Raux, H., Gaudin, Y., Ruigrok, R. W., and Blondel, D. (2005) Nucleocytoplasmic shuttling of the rabies virus P protein requires a nuclear localization signal and a CRM1-dependent nuclear export signal, *Virology 334*, 284−93.
12. Ghildyal, R., Ho, A., Wagstaff, K. M., Dias, M. M., Barton, C. L., Jans, P., Bardin, P., and Jans, D. A. (2005) Nuclear import of the respiratory syncytial virus matrix protein is mediated by importin β1 independent of importin α, *Biochemistry 44*, 12887−95.
13. Chelbi-Alix, M. K., Vidy, A., El Bougrini, J., and Blondel, D. (2006) Rabies viral mechanisms to escape the IFN system: the viral protein P interferes with IRF-3, Stat1, and PML nuclear bodies, *J. Interferon Cytokine Res. 26*, 271−80.
14. Heilman, D. W., Teodoro, J. G., and Green, M. R. (2006) Apoptin nucleocytoplasmic shuttling is required for cell type-specific localization, apoptosis, and recruitment of the anaphase-promoting complex/cyclosome to PML bodies, *J. Virol. 80*, 7535−45.
15. Toriumi, H., Honda, Y., Morimoto, K., Tochikura, T. S., and Kawai, A. (2002) Structural relationship between nucleocapsid-binding activity of the rabies virus phosphoprotein (P) and exposure of epitope 402-13 located at the C terminus, *J. Gen. Virol. 83*, 3035−43.
16. Vidy, A., Chelbi-Alix, M., and Blondel, D. (2005) Rabies virus P protein interacts with STAT1 and inhibits interferon signal transduction pathways, *J. Virol. 79*, 14411−20.
17. Blondel, D., Regad, T., Poisson, N., Pavie, B., Harper, F., Pandolfi, P. P., De The, H., and Chelbi-Alix, M. K. (2002) Rabies virus P and small P products interact directly with PML and reorganize PML nuclear bodies, *Oncogene 21*, 7957−70.
18. Moseley, G. W., Roth, D. M., DeJesus, M. A., Leyton, D. L., Filmer, R. P., Pouton, C. W., Jans, D. A. (2007) Dynein light chain association sequences can facilitate nuclear protein import, *Mol. Biol. Cell* (doi 10.1091/mbc.E07-01-0030).
19. Gupta, A. K., Blondel, D., Choudhary, S., and Banerjee, A. K. (2000) The phosphoprotein of rabies virus is phosphorylated by a unique cellular protein kinase and specific isomers of protein kinase C, *J. Virol. 74*, 91−8.
20. Alvisi, G., Jans, D. A., Guo, J., Pinna, L. A., and Ripalti, A. (2005) A protein kinase CK2 site flanking the nuclear targeting signal enhances nuclear transport of human cytomegalovirus ppUL44, *Traffic 6*, 1002−13.
21. Rosenkranz, A. A., Lunin, V. G., Gulak, P. V., Sergienko, O. V., Shumiantseva, M. A., Voronina, O. L., Gilyazova, D. G., John, A. P., Kofner, A. A., Mironov, A. F., Jans, D. A., and Sobolev,

A. S. (2003) Recombinant modular transporters for cell-specific nuclear delivery of locally acting drugs enhance photosensitizer activity, *FASEB J. 17*, 1121−3.
22. Ho, S. N., Hunt, H. D., Horton, R. M., Pullen, J. K., and Pease, L. R. (1989) Site-directed mutagenesis by overlap extension using the polymerase chain reaction, *Gene 77*, 51−9.
23. Henderson, B. R., and Eleftheriou, A. (2000) A comparison of the activity, sequence specificity, and CRM1-dependence of different nuclear export signals, *Exp. Cell Res. 256*, 213−24.
24. Lam, M. H., Henderson, B., Gillespie, M. T., and Jans, D. A. (2001) Dynamics of leptomycin B-sensitive nucleocytoplasmic flux of parathyroid hormone-related protein, *Traffic 2*, 812−9.
25. Poon, I. K., Oro, C., Dias, M. M., Zhang, J., and Jans, D. A. (2005) Apoptin nuclear accumulation is modulated by a CRM1-recognized nuclear export signal that is active in normal but not in tumor cells, *Cancer Res. 65*, 7059−64.
26. Lam, M. H., Thomas, R. J., Loveland, K. L., Schilders, S., Gu, M., Martin, T. J., Gillespie, M. T., and Jans, D. A. (2002) Nuclear transport of parathyroid hormone (PTH)-related protein is dependent on microtubules, *Mol. Endocrinol. 16*, 390−401.
27. Hubner, S., Xiao, C. Y., and Jans, D. A. (1997) The protein kinase CK2 site (Ser111/112) enhances recognition of the simian virus 40 large T-antigen nuclear localization sequence by importin, *J. Biol. Chem. 272*, 17191−5.
28. Xiao, C. Y., Hubner, S., and Jans, D. A. (1997) SV40 large tumor antigen nuclear import is regulated by the double-stranded DNA-dependent protein kinase site (serine 120) flanking the nuclear localization sequence, *J. Biol. Chem. 272*, 22191−8.
29. Mavrakis, M., McCarthy, A. A., Roche, S., Blondel, D., and Ruigrok, R. W. (2004) Structure and function of the C-terminal domain of the polymerase cofactor of rabies virus, *J. Mol. Biol. 343*, 819−31.
30. Potterton, L., McNicholas, S., Krissinel, E., Gruber, J., Cowtan, K., Emsley, P., Murshudov, G. N., Cohen, S., Perrakis, A., and Noble, M. (2004) Developments in the CCP4 molecular-graphics project, *Acta Crystallogr. D: Biol. Crystallogr. 60*, 2288−94.
31. Chenik, M., Chebli, K., and Blondel, D. (1995) Translation initiation at alternate in-frame AUG codons in the rabies virus phosphoprotein mRNA is mediated by a ribosomal leaky scanning mechanism, *J. Virol. 69*, 707−12.
32. Fornerod, M., Ohno, M., Yoshida, M., and Mattaj, I. W. (1997) CRM1 is an export receptor for leucine-rich nuclear export signals, *Cell 90*, 1051−60.
33. Jacob, Y., Real, E., and Tordo, N. (2001) Functional interaction map of lyssavirus phosphoprotein: identification of the minimal transcription domains, *J. Virol. 75*, 9613−22.
34. la Cour, T., Gupta, R., Rapacki, K., Skriver, K., Poulsen, F. M., and Brunak, S. (2003) NESbase version 1.0: a database of nuclear export signals, *Nucleic Acids Res. 31*, 393−6.
35. Bogerd, H. P., Fridell, R. A., Benson, R. E., Hua, J., and Cullen, B. R. (1996) Protein sequence requirements for function of the human T-cell leukemia virus type 1 Rex nuclear export signal delineated by a novel in vivo randomization−selection assay, *Mol. Cell. Biol. 16*, 4207−14.
36. Craig, E., Zhang, Z. K., Davies, K. P., and Kalpana, G. V. (2002) A masked NES in INI1/hSNF5 mediates hCRM1-dependent nuclear export: implications for tumorigenesis, *EMBO J. 21*, 31−42.
37. Tickenbrock, L., Cramer, J., Vetter, I. R., and Muller, O. (2002) The coiled coil region (amino acids 129−250) of the tumor suppressor protein adenomatous polyposis coli (APC). Its structure and its interaction with chromosome maintenance region 1 (Crm-1), *J. Biol. Chem. 277*, 32332−8.
38. Alefantis, T., Barmak, K., Harhaj, E. W., Grant, C., and Wigdahl, B. (2003) Characterization of a nuclear export signal within the human T cell leukemia virus type I transactivator protein Tax, *J. Biol. Chem. 278*, 21814−22.
39. Murai, N., Murakami, Y., and Matsufuji, S. (2003) Identification of nuclear export signals in antizyme-1, *J. Biol. Chem. 278*, 44791−8.

BI700521M